RSC Advances

PAPER

View Article Online
View Journal | View Issue

Cite this: *RSC Adv.*, 2020, **10**, 11166

Scanning atmospheric-pressure plasma jet treatment of nickel oxide with peak temperature of ~500 °C for fabricating p–i–n structure perovskite solar cells†

Chieh-I. Lin,[ab] Jui-Hsuan Tsai[ab] and Jian-Zhang Chen *[ab]

Received 26th November 2019
Accepted 11th March 2020

DOI: 10.1039/d0ra01434f

rsc.li/rsc-advances

Scanning atmospheric-pressure plasma jet (APPJ) treatment of nickel oxide with a peak temperature of 500 °C was performed for fabricating p–i–n structure perovskite solar cells (PSCs). APPJ post-treatment increases the haze of NiO on FTO glass, leading to enhanced light scattering in PSCs that in turn improves the cell efficiency. APPJ treatment on NiO also improves the wettability to facilitate the follow-up deposition of $CH_3NH_3PbI_3$. This also leads to better PSC performance. X-ray photoelectron spectroscopy indicates that APPJ treatment results in fewer C–N bonds and reduced $NiAc_2$ content, suggesting more complete conversion of the liquid precursor into NiO. With three APPJ scans, the average PCE improves from 11.91% to 13.47%, with the best-performing PSC achieving an efficiency of 15.67%.

1. Introduction

Recently, organic–inorganic hybrid perovskite solar cells (PSCs) have been developed rapidly owing to their excellent properties.[1–5] The power conversion efficiency (PCE) of PSCs has been improved rapidly to 25.2%[6–10] within a decade. In fact, their PCE exceeds that of CIGS- and CdTe-based solar cells and is already comparable to that of Si-based single-junction solar cells.[11,12]

The hole transport layer (HTL) plays important roles in hole collection, hole transportation, and electron-blocking; therefore, optimizing the HTL for matching energy levels, enhancing light transmittance, and improving interfacial compatibility is essential for realizing good PSCs. NiO is a widely used HTL for a p–i–n PSC. NiO has a high work function (~5.1 eV) and deep valence band (~5.4 eV). Furthermore, it is chemically more stable compared with poly(3,4-ethylenedioxythiophene)-poly(styrenesulfonate) (PEDOT:PSS). Typical deposition techniques used for NiO are sol–gel process,[13,14] sputtering,[15,16] pulsed laser deposition,[17,18] and spray pyrolysis.[19,20] The fill factor (F.F.) and short circuit current (J_{sc}) of PSCs with an NiO HTL were reported to be relatively low owing to the lower conductivity of NiO and poor contact between NiO and the perovskite layer. To overcome these problems, surface modification and doping are investigated to improve the performance of a PSC with an NiO HTL. Ag, Cu, Li, and Cs are the typical dopants introduced to NiO for improving its p-type conductivity and band alignment;[21–26] interfacial modification is also applied to improve PSC performance.[27]

Low-pressure plasma (LPP) has been widely applied in industry for thin-film deposition and etching. However, generating LPP requires vacuum chamber and vacuum pumps that are costly and require routine maintenance. It is also disadvantageous to integrate with non-vacuum device fabrication procedures and roll-to-roll processes. By contrast, atmospheric-pressure plasma (APP) can be operated at a regular pressure and has shown promise in applications such as clinical medication, agriculture, and materials syntheses and surface modification.[28–31] Typical APP technology includes gliding arc, corona discharge, dielectric barrier discharge, and atmospheric pressure plasma jet (APPJ). Recent developments have resolved problems such as continuous arcing, high breakdown voltage, and instability.[32–34] APPJ with medium temperature (400–700 °C) has demonstrated rapid materials processing capability owing to the synergetic effect of reactive plasma species and heat.[35–38]

In this study, a scan-mode nitrogen DC-pulse APPJ is used to treat NiO for PSCs. The peak temperature of the substrate during APPJ operation is ~500 °C. The optical transmittance, haze spectra, surface morphology, chemical bonding configuration, wettability, conductivity, and electrochemical properties of scanning APPJ-treated NiO are characterized. PSCs with scanning APPJ-treated NiO also show improved performance compared to samples with only 10 min hot plate treatment, with

[a]*Graduate Institute of Applied Mechanics, National Taiwan University, Taipei City 10617, Taiwan. E-mail: jchen@ntu.edu.tw*

[b]*Advanced Research Center for Green Materials Science and Technology, National Taiwan University, Taipei City 10617, Taiwan*

† Electronic supplementary information (ESI) available. See DOI: 10.1039/d0ra01434f

PCE increasing from 11.91% to 13.47%; J_{sc} from 16.96 mA to 17.55 mA cm^{-2}; and F.F. from 68.56% to 73.66%.

2. Experimental section

2.1. Fabrication of PSC

Deionized water, acetone, and isopropanol were used sequentially to rinse the FTO glass substrate (TEC7, ~8 Ω sq^{-1}) with ultrasonication for 15 min each. Next, the FTO substrate was treated by UV–ozone for 15 min. The precursor solution for the NiO film was prepared with 0.5 M nickel acetate (99.998%, trace metal basis, Sigma-Aldrich) and ethanolamine (99.5%, Sigma-Aldrich) dissolved in ethanol; the solution was stirred overnight at 60 °C.[39] A liquid precursor film was spin-coated on the FTO glass substrate for 40 s at 6000 rpm, following which the liquid-precursor-film-coated sample was calcined at 325 °C for 10 min for APPJ-treated NiO samples. The thickness of the resultant NiO was ~30 nm. An NiO thin-film-coated FTO glass substrate was thus obtained. After natural cooing to room temperature, the NiO film was treated by a nitrogen APPJ in scanning mode three times. The counterpart samples without APPJ treatment on NiO films were calcined at 325 °C on a hot plate for 10 and 90 min. Next, we transferred the samples into a nitrogen-filled glove box immediately for follow-up $CH_3NH_3PbI_3$ depositions. The perovskite film was deposited by a one-step process. The $CH_3NH_3PbI_3$ solution included 1.2 mM CH_3NH_3I (MAI, 98%, Dyesol) and PbI_2 (99.999%, trace metal basis, Alfa Aesar) dissolved in dimethylformamide (DMF, 99.8%, Sigma-Aldrich). The resultant solution was spin-coated on NiO at 5000 rpm for 30 s; during the spin-coating process, 200 μl of CB was dripped rapidly onto the sample after starting spinning for 7 s. Next, the sample was calcined at 100 °C for 10 min to form a dense perovskite film (thickness: ~350 nm). $PC_{61}BM$ (nano-C, 20 mg ml^{-1} in chlorobenzene) was doped with 2 μl of *N*,*N*-dimethyl-*N*-octadecyl(3-aminopropyl)trimethoxysilyl chloride silane (DMOAP, Sigma-Aldrich, 42 wt% in methanol). The DMOAP-doped $PC_{61}BM$ solution was spin-coated at 2000 rpm for 30 s.[40] Then, bathocuproine (BCP, Alfa Aesar, 0.5 mg ml^{-1} in 2-propanol) was spin-coated at 6000 rpm for 20 s, following which it was dried at 85 °C for 15 min. Finally, 85 nm-thick Ag with area of 0.09 cm^2 was deposited on the sample using an e-beam evaporator.

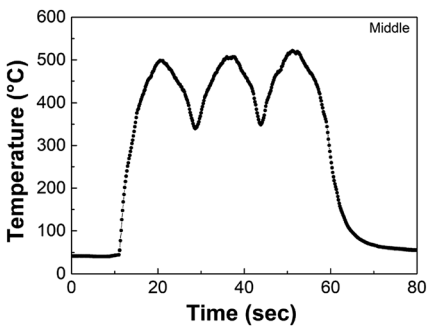

Fig. 1 Temperature evolution of substrate under APPJ operation.

2.2. APPJ treatment on NiO

Fig. S1† shows the schematic of the APPJ equipment used in this study. The NiO film was first annealed at 325 °C for 10 min, following which it was treated by an APPJ in scanning mode three times with a scanning speed of 0.2 cm s^{-1}. The details of the APPJ system are described elsewhere.[41] A Pyrex™ tube with 4.8 cm length with 3 cm internal diameter was installed downstream of the plasma jet; the end of this tube was ~1 mm

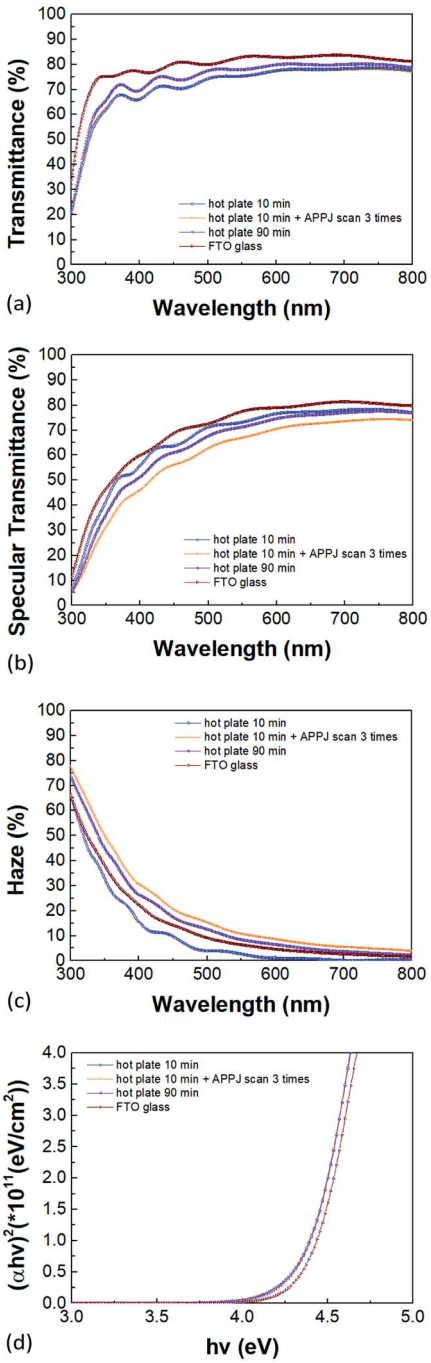

Fig. 2 UV-vis spectra of NiO film on FTO glass: (a) total transmittance spectra, (b) specular transmittance spectra, (c) haze spectra and (d) Tauc plot.

above the substrate. This tube is used for minimizing the ambient air-quenching effect while allowing the high-rate gas to flow out smoothly. APPJ operation was performed with N_2 flow rate of 46 slm to realize peak substrate temperature of 500 °C. Fig. 1 shows the representative temperature evolution of the FTO glass during three APPJ scans. The peak temperature is set to be ~500 °C by adjusting the tube length and flow rate. The temperature was measured by a K-type thermocouple. The counterpart samples without APPJ treatment on NiO films were calcined at 325 °C on a hot plate for 10 and 90 min.

2.3. Characterization of NiO films and PSCs

The surface morphology of NiO was examined using scanning electron microscopy (SEM, JOEL, JSM-7800Prime) and atomic force microscopy (AFM, Bruker, BioScope Resolve). The ultraviolet-visible (UV-vis) transmittance and reflectance were measured by a UV-vis spectrophotometer (JASCO, V-670), and the through-plane (perpendicular to the film surface) conductivity was measured by an electrometer (Keithley 2636A). The sample for conductivity measurement was FTO glass/NiO/Ni structure, in which Ni was used for ohmic contact. A contact angle goniometer (Sindatek, Model 100SB) was used to measure the water contact angle. The surface chemical bonding status and elemental composition were analyzed using X-ray photoelectron spectroscopy (XPS, Thermo Fisher Scientific, ESCALAB Xi^+). The Current density–voltage (*J–V*) curves of the PSC were measured using a sourcemeter (Agilent, B2902A) under illumination of simulated AM1.5 light (ABET, Sun 2000 Solar Simulator). For *J–V* curves, both forward and reverse scans were measured and forward scan was measured first. Electrochemical impedance spectroscopy was performed using an electrochemical workstation (EIS, Metrohm-Autolab, PGSTAT204) from 1 MHz to 1 Hz.

3. Results and discussion

Fig. 2(a) shows the total transmittance spectra; the total transmittance remains similar after the APPJ treatment. Fig. 2(b) and (c) show plots of the specular transmittance and haze spectra, respectively. The specular transmittance reduced after APPJ treatment. The haze was calculated as[42]

$$\text{Haze} = \frac{T_t - T_s}{T_t} \times 100\% \quad (1)$$

where T_t is the total transmittance and T_s, the specular transmittance. The two total transmittance curves, for the samples with bare 10 min hot plate calcination and 10 min hot plate plus three APPJ scans, almost overlap with only ~1% difference. APPJ treatment apparently increased the haze of the NiO coated FTO. This could increase the forward light scattering as light passes through the NiO-coated FTO. Fig. 2(d) shows the Tauc bandgap that is calculated as[43]

$$(\alpha h\nu)^n = A(h\nu - E_g) \quad (2)$$

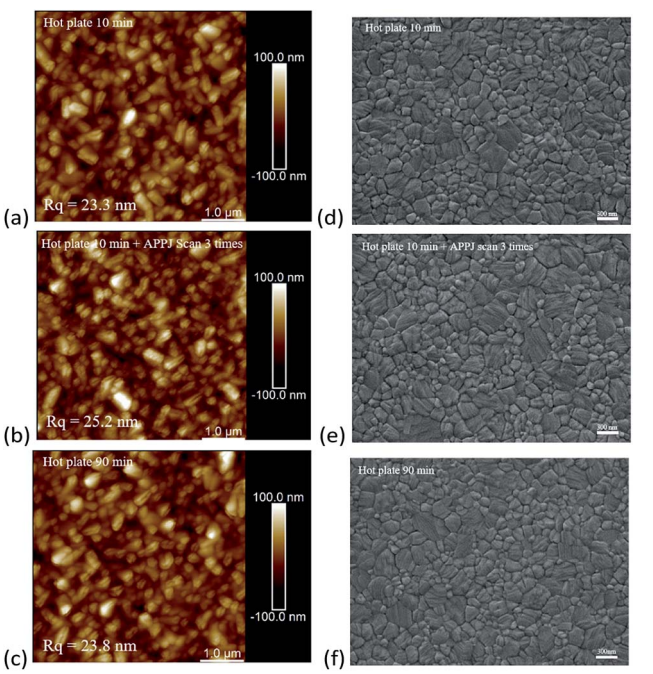

Fig. 3 AFM images of FTO/NiO structure (a–c) and SEM of FTO/NiO/$CH_3NH_3PbI_3$ structure (d–f) with NiO (a and d) 10 min hot plate treatment, (b and e) 10 min hot plate plus three APPJ scans, and (c and f) 90 min hot plate treatment.

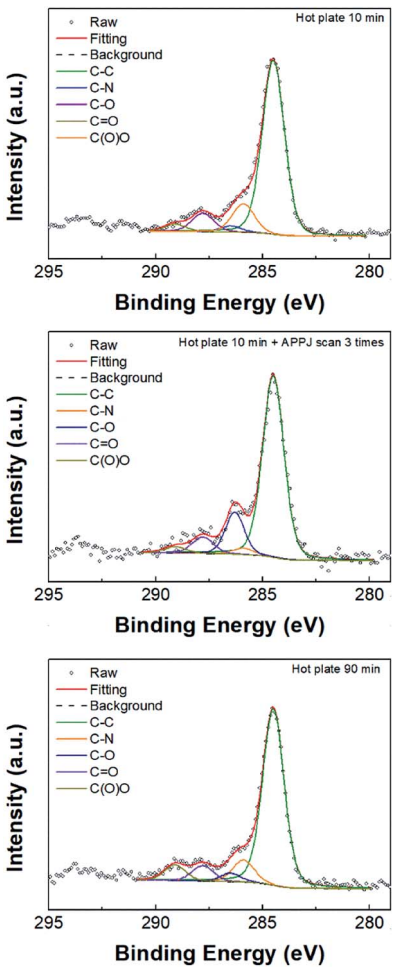

Fig. 4 XPS C 1s spectra of NiO film with different treatment.

where α is the absorption coefficient; A, a constant; $h\nu$, the photon energy; and E_g, the optical bandgap; further, $n = 2$ refers to the direct bandgap of NiO. The measured band gap was ~4.37 eV; this agrees with the previously reported data.[25,44]

The surface coverage and crystallinity of the perovskite layer have been reported to be pivotal for the device performance.[45] Fig. 3(a)–(c) show the AFM measurement results for NiO-coated FTO under different NiO treatment conditions and Fig. 3(d)–(f) show the corresponding SEM measurement results of $CH_3NH_3PbI_3$ coated NiO on FTO. After APPJ treatment, the roughness increased from ~23 nm to ~25 nm. This could enhance the forward light scattering to improve the cell efficiency,[13,46] thus agreeing well with the haze spectra shown in Fig. 2(c). Fig. 3(d)–(f) show SEM images of the $CH_3NH_3PbI_3$ films. The $CH_3NH_3PbI_3$ films are dense and well-crystallized. Fig. S2† shows SEM images of cross sections of the films; the films look compact in these views.

Fig. 4 and 5 show the XPS C 1s and Ni $2p_{3/2}$ binding energy spectra for NiO films. The C–C bond peak was adjusted to 284.5 eV; the main peaks for C 1s are located at 284.5, 285.9, 286.5, 287.8, and 289.1, and they respectively correspond to C–C, C–N, C–O, C=O, and C(O)O.[47,48] The C–N bond can be ascribed to the ethanolamine residue (left from liquid precursor) after calcination. Table S1† shows the deconvoluted peak areal fractions. After APPJ treatment, the C–N content decreased significantly; simultaneously, the C–O content increased. As for the Ni

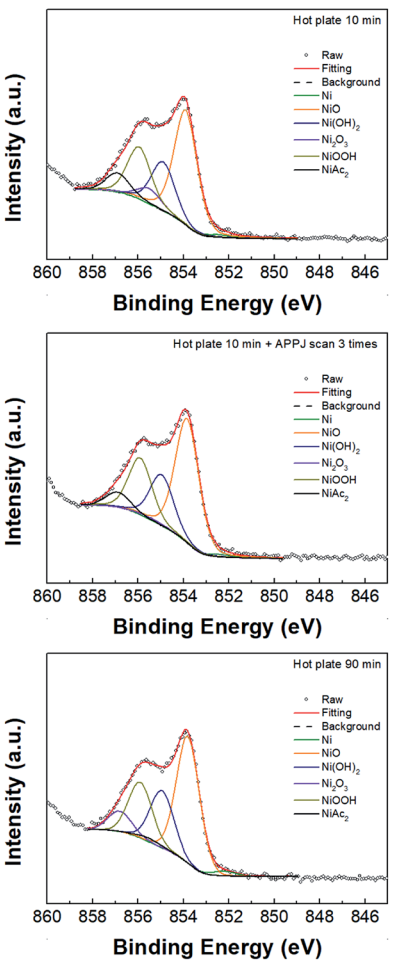

Fig. 5 XPS Ni $2p_{3/2}$ spectra of NiO film with different treatment.

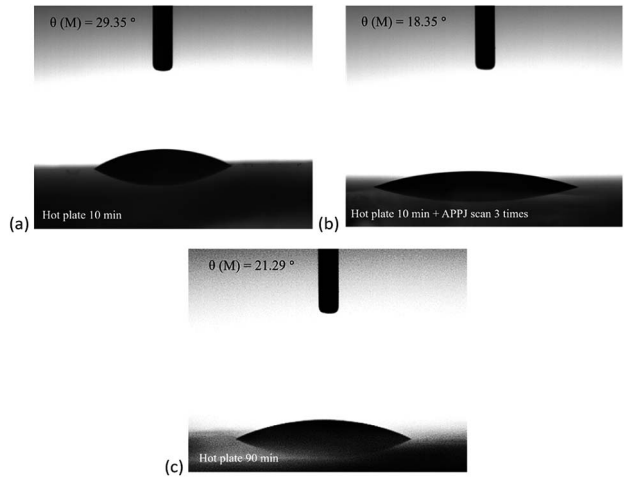

Fig. 6 Water contact angles of NiO films with (a) 10 min hot plate treatment, (b) 10 min hot plate and three APPJ scans, and (c) 90 min hot plate treatment.

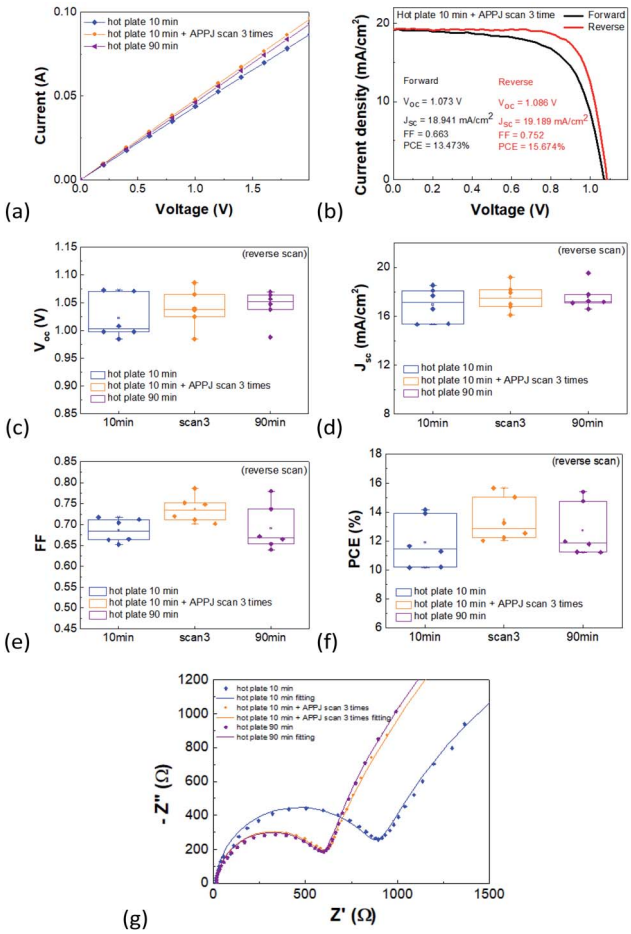

Fig. 7 (a) Current–voltage curve (conductivity) measured through NiO plane. (b) J–V curves of the best-achieving PSC. Statistical plots for (c) V_{oc}, (d) J_{sc}, (e) FF, and (f) PCE for six batches of PSCs. (g) Nyquist plots for EIS measurement.

Table 1 PV parameters of PSCs

	V_{oc} (V)	J_{sc} (mA cm^{-2})	FF	PCE (%)
Hot plate 10 min	1.02 ± 0.04	16.96 ± 1.38	68.56 ± 3.24	11.91 ± 1.76
Hot plate 10 min + three APPJ scans	1.04 ± 0.03	17.55 ± 1.11	73.66 ± 5	13.47 ± 1.54
Hot plate 90 min	1.04 ± 0.03	17.59 ± 1.03	69.09 ± 5.50	12.74 ± 1.86

Table 2 EIS

	R_1 (Ω)	R_2 (Ω)	CPE2-T (F)	CPE2-P	R_3 (Ω)	CPE3-T (F)	CPE3-P
Hot plate 10 min	16.87	743.9	6.930×10^{-9}	1	4930	3.6265×10^{-6}	0.73
Hot plate 10 min + three APPJ scans	17.64	558.1	6.71×10^{-9}	1	8052	1.4596×10^{-6}	0.82
Hot plate 90 min	19.19	557.9	6.550×10^{-9}	1	6864	1.1682×10^{-6}	0.85

$2p_{3/2}$ spectra (Fig. 5), the main peaks at 852.2, 853.8, 855, 855.4, 855.8, and 856.8 respectively correspond to Ni, NiO, $Ni(OH)_2$, $NiAc_2$, NiOOH and Ni_2O_3.[10,49,50] Table S2† lists the areal fractions of deconvoluted peaks. The sample subjected to 10 min hot plate treatment shows relatively high $NiAc_2$ content owing to the incomplete transformation of the liquid precursor into the NiO film. Similar phenomena were also observed in other studies.[13,39] After APPJ treatment, the NiO content increased and $NiAc_2$ content apparently decreased, suggesting that APPJ treatment can further convert precursor residue into NiO.

Fig. 6 shows the water contact measurement results. The water contact angle of 10 min hot plate treated NiO was ~29°. After APPJ treatment, the water contact angle decreased to ~18°. In comparison, the water contact angle of 90 min hot plate treated NiO was ~21°. The wettability of NiO could influence the grain size and crystallinity of the follow-up deposited $CH_3NH_3PbI_3$. These, in turn, will change the trap density of the $CH_3NH_3PbI_3$ film.[51–53]

Fig. 7(a) shows the through-plane conductivity of the NiO films. APPJ treatment slightly increased the NiO conductivity from 1.98×10^{-3} mS cm^{-1} to 2.10×10^{-3} mS cm^{-1}. It is speculated that a higher amount of ethanolamine residue results in reduced NiO film conductivity, as evidenced in the XPS experiment. Fig. 7(b) shows the *J–V* curves of the best-performing PSC with 10 min hot plate treatment and three APPJ scans. The PSC efficiency reached 15.67%. Fig. 7(c)–(f) shows statistical plots of the photovoltaic parameters of six batches of PSCs and Table 1 lists the corresponding statistics of PV parameters for reverse scans. As shown in Table 1, the PSC with NiO subjected to 10 min hot plate and three APPJ scans exhibited the highest average J_{sc}, F.F. and PCE; these parameters improved from 16.96 mA cm^{-2}, 68.56%, and 11.91% to 17.55 mA cm^{-2}, 73.66%, and 13.47%, respectively. The increased F.F. and J_{sc} can be attributed to the increased haze of NiO on FTO, improved wettability, and increased through-plane conductivity. The PSC performance with APPJ treatment also surpasses those with 90 min hot plate treatment. This indicates that APPJ treatment can improve the PSC performance with less processing time.

EIS measurements were also performed under illumination to investigate the internal charge transporting and recombination through the devices.[54] Fig. S3† shows the fitting model circuit.[55] Fig. 7(g) shows the Nyquist plot with the fitting parameters listed in Table 2. R_1, R_2, and R_3 represent the series resistance, charge transporting resistance, and recombination resistance, respectively. Clearly, R_2 decreased (lower charge transport resistance) after APPJ treatment due to the higher surface roughness and conductivity. Further, the enhanced wettability of NiO with APPJ treatment may enhance the crystallinity of the follow-up $CH_3NH_3PbI_3$ with lower grain boundaries and trap densities, thereby inhibiting the non-radiative recombination related to R_3.

4. Summary

Scanning APPJ treatment on NiO with peak temperature of 500 °C can improve the performance of p–i–n PSCs. APPJ treatment increases the haze of the NiO film, leading to the improved forward light scattering that in turn improves the efficiency of the PSC. APPJ treatment could also improve the wettability of NiO to facilitate the follow-up deposition of $CH_3NH_3PbI_3$. XPS shows fewer C–N bonds and $NiAc_2$ content after APPJ treatment, indicating enhanced conversion of the liquid precursor conversion into NiO. A PSC with NiO subjected to 10 min hot plate and three APPJ scans exhibited the highest average J_{sc}, F.F. and PCE; these parameters improved from 16.96 mA cm^{-2}, 68.56%, and 11.91% to 17.55 mA cm^{-2}, 73.66%, and 13.47%, respectively.

Conflicts of interest

There are no conflicts to declare.

Acknowledgements

We gratefully acknowledge the funding support from the Ministry of Science and Technology of Taiwan under grant no. MOST 108-2221-E-002-088-MY3. This work is also financially supported by the "Advanced Research Center for Green Materials Science and Technology" from the Featured Area Research Center Program of the Higher Education Sprout Project by the

Ministry of Education (108L9006) and the Ministry of Science and Technology in Taiwan (MOST 108-3017-F-002-002). We would like to specially thank Ms. Yuan-Tze Lee for her help with the SEM operation. The facility support from the Nano-Electro-Mechanical-Systems (NEMS) Research Center at National Taiwan University, Taiwan is also gratefully acknowledged.

Notes and references

1 P. Gao, M. Gratzel and M. K. Nazeeruddin, *Energy Environ. Sci.*, 2014, **7**, 2448–2463.
2 P. P. Boix, K. Nonomura, N. Mathews and S. G. Mhaisalkar, *Mater. Today*, 2014, **17**, 16–23.
3 H. Choi, J. Jeong, H. B. Kim, S. Kim, B. Walker, G. H. Kim and J. Y. Kim, *Nano Energy*, 2014, **7**, 80–85.
4 A. Kojima, K. Teshima, Y. Shirai and T. Miyasaka, *J. Am. Chem. Soc.*, 2009, **131**, 6050–6051.
5 Q. Dong, Y. Fang, Y. Shao, P. Mulligan, J. Qiu, L. Cao and J. J. Huang, *Science*, 2015, **347**, 967–970.
6 S. Ryu, J. Seo, S. S. Shin, Y. C. Kim, N. J. Jeon, J. H. Noh and S. I. Seok, *J. Mater. Chem. A*, 2015, **3**, 3271–3275.
7 J. Burschka, N. Pellet, S. J. Moon, R. Humphry-Baker, P. Gao, M. K. Nazeeruddin and M. Gratzel, *Nature*, 2013, **499**, 316–319.
8 M. L. Jiang, J. M. Wu, F. Lan, Q. Tao, D. Gao and G. Y. Li, *J. Mater. Chem. A*, 2015, **3**, 963–967.
9 M. M. Lee, J. Teuscher, T. Miyasaka, T. N. Murakami and H. J. Snaith, *Science*, 2012, **338**, 643–647.
10 Z. A. Tan, W. Q. Zhang, D. P. Qian, C. H. Cui, Q. Xu, L. J. Li, S. S. Li and Y. F. Li, *Phys. Chem. Chem. Phys.*, 2012, **14**, 14217–14223.
11 National Renewable Energy Laboratory, https://www.nrel.gov/pv/cell-efficiency.html.
12 M. Salado, L. Contreras-Bernal, L. Calio, A. Todinova, C. Lopez-Santos, S. Ahmad, A. Borras, J. Idigoras and J. A. Anta, *J. Mater. Chem. A*, 2017, **5**, 10917–10927.
13 Z. L. Zhu, Y. Bai, T. Zhang, Z. K. Liu, X. Long, Z. H. Wei, Z. L. Wang, L. X. Zhang, J. N. Wang, F. Yan and S. H. Yang, *Angew. Chem., Int. Ed.*, 2014, **53**, 12571–12575.
14 Z. J. Hu, D. Chen, P. Yang, L. J. Yang, L. S. Qin, Y. X. Huang and X. C. Zhao, *Appl. Surf. Sci.*, 2018, **441**, 258–264.
15 K. C. Wang, P. S. Shen, M. H. Li, S. Chen, M. W. Lin, P. Chen and T. F. Guo, *ACS Appl. Mater. Interfaces*, 2014, **6**, 11851–11858.
16 J. Cui, F. P. Meng, H. Zhang, K. Cao, H. L. Yuan, Y. B. Cheng, F. Huang and M. K. Wang, *ACS Appl. Mater. Interfaces*, 2014, **6**, 22862–22870.
17 Z. W. Qiu, H. B. Gong, G. H. J. Zheng, S. A. Yuan, H. L. Zhang, X. M. Zhu, H. P. Zhou and B. Q. Cao, *J. Mater. Chem. C*, 2017, **5**, 7084–7094.
18 J. H. Park, J. Seo, S. Park, S. S. Shin, Y. C. Kim, N. J. Jeon, H. W. Shin, T. K. Ahn, J. H. Noh, S. C. Yoon, C. S. Hwang and S. I. Seok, *Adv. Mater.*, 2015, **27**, 4013–4019.
19 Y. S. Qin, J. Song, Q. Y. Qiu, Y. Liu, Y. L. Zhao, L. Zhu and Y. H. Qiang, *J. Alloys Compd.*, 2019, **810**, 151970.
20 K. O. Ukoba, A. C. Eloka-Eboka and F. L. Inambao, *Renewable Sustainable Energy Rev.*, 2018, **82**, 2900–2915.
21 W. Chen, F. Z. Liu, X. Y. Feng, A. B. Djurisic, W. K. Chan and Z. B. He, *Adv. Energy Mater.*, 2017, **7**, 1700722.
22 K. Yao, F. Li, Q. Q. He, X. F. Wang, Y. H. Jiang, H. T. Huang and A. K. Y. Jen, *Nano Energy*, 2017, **40**, 155–162.
23 J. W. Jung, C. C. Chueh and A. K. Y. Jen, *Adv. Mater.*, 2015, **27**, 7874–7880.
24 T. Dutta, P. Gupta, A. Gupta and J. Narayan, *J. Appl. Phys.*, 2010, **108**, 083715.
25 J. Zheng, L. Hu, J. S. Yun, M. Zhang, C. F. J. Lau, J. Bing, X. Deng, Q. Ma, Y. Cho and W. J. Fu, *ACS Appl. Energy Mater.*, 2018, **1**, 561–570.
26 L. Xu, X. F. Chen, J. J. Jin, W. Liu, B. Dong, X. Bai, H. W. Song and P. Reiss, *Nano Energy*, 2019, **63**, 103860.
27 Q. F. Xue, Y. Bai, M. Y. Liu, R. X. Xia, Z. C. Hu, Z. M. Chen, X. F. Jiang, F. Huang, S. H. Yang, Y. Matsuo, H. L. Yip and Y. Cao, *Adv. Energy Mater.*, 2017, **7**, 1602333.
28 T. von Woedtke, H. R. Metelmann and K. D. Weltmann, *Contrib. Plasma Phys.*, 2014, **54**, 104–117.
29 S. H. Yang, C. H. Liu, C. H. Su and H. Chen, *Thin Solid Films*, 2009, **517**, 5284–5287.
30 M. J. Shenton and G. C. Stevens, *J. Phys. D: Appl. Phys.*, 2001, **34**, 2761–2768.
31 O. V. Penkov, M. Khadem, W. S. Lim and D. E. Kim, *J. Coat. Technol. Res.*, 2015, **12**, 225–235.
32 R. Brandenburg, *Plasma Sources Sci. Technol.*, 2017, **26**, 053001.
33 M. Laroussi and T. Akan, *Plasma Processes Polym.*, 2007, **4**, 777–788.
34 J. Winter, R. Brandenburg and K. D. Weltmann, *Plasma Sources Sci. Technol.*, 2015, **24**, 064001.
35 H. M. Chang, Y. J. Yang, H. C. Li, C. C. Hsu, I. C. Cheng and J. Z. Chen, *J. Power Sources*, 2013, **234**, 16–22.
36 H. W. Liu, S. P. Liang, T. J. Wu, H. M. Chang, P. K. Kao, C. C. Hsu, J. Z. Chen, P. T. Chou and I. C. Cheng, *ACS Appl. Mater. Interfaces*, 2014, **6**, 15105–15112.
37 C. H. Xu, P. Y. Shen, Y. F. Chiu, P. W. Yeh, C. C. Chen, L. C. Chen, C. C. Hsu, I. C. Cheng and J. Z. Chen, *J. Alloys Compd.*, 2016, **676**, 469–473.
38 F. H. Kuok, C. Y. Liao, T. H. Wan, P. W. Yeh, I. C. Cheng and J. Z. Chen, *J. Alloys Compd.*, 2017, **692**, 558–562.
39 J.-H. Tsai, S.-M. Hsu, I.-C. Cheng, C.-C. Hsu and J.-Z. Chen, *Ceram. Int.*, 2019, **45**, 22078–22084.
40 J. H. Tsai, I. C. Cheng, C. C. Hsu, C. C. Chueh and J. Z. Chen, *Electrochim. Acta*, 2019, **293**, 1–7.
41 Y. W. Hsu, H. C. Li, Y. J. Yang and C. C. Hsu, *Thin Solid Films*, 2011, **519**, 3095–3099.
42 A. Nirmal, A. K. K. Kyaw, X. W. Sun and H. V. Demir, *Opt. Express*, 2014, **22**, A1412–A1421.
43 N. P. Klochko, V. R. Kopach, I. I. Tyukhov, D. O. Zhadan, K. S. Klepikova, G. S. Khrypunov, S. I. Petrushenko, V. M. Lyubov, M. V. Kirichenko, S. V. Dukarov and A. L. Khrypunova, *Sol. Energy*, 2018, **164**, 149–159.
44 Z. Zhai, X. Huang, M. Xu, J. Yuan, J. Peng and W. J. Ma, *Adv. Energy Mater.*, 2013, **3**, 1614–1622.
45 P. W. Liang, C. Y. Liao, C. C. Chueh, F. Zuo, S. T. Williams, X. K. Xin, J. Lin and A. K. Jen, *Adv. Mater.*, 2014, **26**, 3748–3754.

46 Y. J. Xia, K. Sun, J. J. Chang and J. Y. Ouyang, *J. Mater. Chem. A*, 2015, **3**, 15897–15904.
47 S. Stankovich, R. D. Piner, X. Q. Chen, N. Q. Wu, S. T. Nguyen and R. S. Ruoff, *J. Mater. Chem.*, 2006, **16**, 155–158.
48 S. Stankovich, D. A. Dikin, R. D. Piner, K. A. Kohlhaas, A. Kleinhammes, Y. Jia, Y. Wu, S. T. Nguyen and R. S. Ruoff, *Carbon*, 2007, **45**, 1558–1565.
49 S. Liu, R. Liu, Y. Chen, S. Ho, J. H. Kim and F. J. So, *Chem. Mater.*, 2014, **26**, 4528–4534.
50 M. Kitao, K. Izawa, K. Urabe, T. Komatsu, S. Kuwano and S. J. Yamada, *Jpn. J. Appl. Phys.*, 1994, **33**, 6656.
51 Z. G. Xiao, Y. B. Yuan, Q. Wang, Y. C. Shao, Y. Bai, Y. H. Deng, Q. F. Dong, M. Hu, C. Bi and J. S. Huang, *Mater. Sci. Eng. R Rep.*, 2016, **101**, 1–38.
52 Q. Wang, C. C. Chueh, T. Zhao, J. Cheng, M. Eslamian, W. C. H. Choy and A. K. Y. Jen, *Chemsuschem*, 2017, **10**, 3794–3803.
53 N. K. Noel, A. Abate, S. D. Stranks, E. S. Parrott, V. M. Burlakov, A. Goriely and H. J. Snaith, *ACS Nano*, 2014, **8**, 9815–9821.
54 V. Gonzalez-Pedro, E. J. Juarez-Perez, W. S. Arsyad, E. M. Barea, F. Fabregat-Santiago, I. Mora-Sero and J. Bisquert, *Nano Lett.*, 2014, **14**, 888–893.
55 Z. H. Liu, A. L. Zhu, F. S. Cai, L. M. Tao, Y. H. Zhou, Z. X. Zhao, Q. Chen, Y. B. Cheng and H. P. Zhou, *J. Mater. Chem. A*, 2017, **5**, 6597–6605.